PHYSICAL REVIEW B **74**, 081403(R) (2006)

Phase diagram for the Ni/Al_2O_3 interface and relationships to adhesion

X.-G. Wang,[1] J. R. Smith,[1] and A. G. Evans[2]
[1]*Delphi Research Labs, Shelby Township, Michigan 48315, USA*
[2]*University of California, Santa Barbara, California 93106, USA*
(Received 25 April 2006; published 23 August 2006)

First-principles calculations conducted over a broad range of atomic configurations have been used to determine the phase diagram and work of separation for Ni/Al_2O_3 interfaces. Seven interfacial phases have been identified. The results reveal that the strongest (O-rich) phases derive their strength from ionic Ni-O bonds across the interface, reminiscent of NiO. The Al-rich phases are also strong, exhibiting a mix of Ni_3Al-like and Al_2O_3-like interfacial bonds. The stoichiometric interfaces are the weakest since they are formed from the ground-state $Al_2O_3(0001)$ surface.

DOI: 10.1103/PhysRevB.74.081403 PACS number(s): 68.35.Ct

The Ni/Al_2O_3 interface has been the subject of considerable research because of its importance for hot-section turbine components, such as airfoils for aircraft propulsion and power generation.[1–5] In hot-section components, this interface develops by Al_2O_3 forming as a thermally grown oxide between a Ni(Al) alloy bond coat and a ZrO_2 thermal barrier. The Al_2O_3 acts as an oxygen-diffusion barrier, protecting the underlying superalloy from oxidation. The durability of these systems is often dictated by the stability or adhesion of the Ni/Al_2O_3 interface. It is therefore important to identify and quantify the fundamental properties affecting this adhesion. One objective of this article is to present first-principles computations of the Ni/Al_2O_3 interfacial phases, expressed as an interfacial diagram, in a space comprising the temperature and Al activity. Another is to calculate the interfacial adhesion for each of the phases.

The research to be reported embellishes previous assessments of the work of separation, W_{sep},[6] defined as the total energy of the fully separated solids minus the total energy at their equilibrium separation, per unit area. It is the appropriate metric for analyzing fracture, where bond separation rates are sufficiently high that the surfaces cannot relax to the ground state before they are separated. Another quantity of interest is the work of adhesion, W_{ad}, obtained by allowing all the surfaces to relax to the ground state, as in sessile drop experiments. This prior research[6] ascertained the importance of the Al_2O_3-terminating layer at the interface. Specifically, oxygen-terminated interfaces provided high W_{sep}, while stoichiometric interfaces resulted in low W_{sep}. The effects of S segregation and the consequent reduction in adhesion have also been computed.[11] Similar features calculated for the Cu/Al_2O_3 interface[6] have been substantiated experimentally.[7–10] In these assessments, $Al_2O_3(0001)$ was used. The Al-rich interface was represented by an $Al_2O_3(0001)$ termination of two Al atomic layers ($n_{Al}/n_O=1$), the O-rich interface by one O atomic layer($n_{Al}/n_O=1/3$), and the stoichiometric interface by a single Al atomic layer ($n_{Al}/n_O=2/3$). These original studies had the deficiency that, because of limited computational capability, they did not fully characterize the interfacial phases as functions of temperature and Al activity, nor did they establish the full phase dependence of W_{sep} at the atomic level. With the availability of more advanced computer resources, a broader set of interfacial configurations can now be tested, allowing for interfacial atomic mixing, vacancy formation, and corresponding stoichiometry variations. Interfaces that allow these phenomena could deviate from the model $Al_2O_3(0001)$ terminations. Ascertaining these phases is the objective of the present assessment.

The $Ni(111)/Al_2O_3(0001)$ orientation relationship has been chosen to be consistent with experimental observations.[12,13] As reference, we use the oxygen-rich phase formed by termination of the $Al_2O_3(0001)$ at an oxygen atomic layer. The Gibbs free energy of formation ΔG for interfacial phase x relative to the reference phase is given as

$$\Delta G = G_x - G_{\mathrm{ref}} + \Delta N_{\mathrm{Ni}}\mu_{\mathrm{Ni}} + \Delta N_{\mathrm{Al}}\mu_{\mathrm{Al}} + \Delta N_{\mathrm{O}}\mu_{\mathrm{O}}. \quad (1)$$

Here G_x is the free energy for the Ni/Al_2O_3 interfacial phase x and G_{ref} that for the reference phase. The quantities ΔN_{Ni}, ΔN_{Al}, and ΔN_{O} represent differences in the numbers of Ni, Al, and O atoms, respectively, between the interfacial and reference phases: while μ_{Ni}, μ_{Al}, and μ_{O} are the chemical potentials of Ni, Al, and O, respectively. Equation (1) can also be written as

$$\Delta G = G_x - G_{\mathrm{ref}} + \Delta N_{\mathrm{Ni}}\mu_{\mathrm{Ni}} + [\Delta N_{\mathrm{Al}} - (2/3)N_{\mathrm{O}}]\mu_{\mathrm{Al}} + (1/3)\Delta N_{\mathrm{O}}\mu_{\mathrm{Al_2O_3}}, \quad (2)$$

where

$$\mu_{\mathrm{Al_2O_3}} = 2\mu_{\mathrm{Al}} + 3\mu_{\mathrm{O}},$$

and

$$G_x - G_{\mathrm{ref}} = E_x^{total} - E_{\mathrm{ref}}^{\mathrm{total}} + P\Delta V + \Delta F_{\mathrm{s}}(T). \quad (3)$$

Here $E_{\mathrm{x}}^{\mathrm{total}}$ and $E_{\mathrm{ref}}^{\mathrm{total}}$ are the total energies of the phase x and the reference phase, respectively, at 0 K. The volume difference between the two phases is ΔV, with P the pressure and ΔF_{s} the free energy difference due to vibrational contributions. The $P\Delta V$ and ΔF_{s} terms are small compared with $E_{\mathrm{x}}^{\mathrm{total}} - E_{\mathrm{ref}}^{\mathrm{total}}$ (Refs. 14–18) and are therefore not included. Connection to the metallurgical variable of choice, the Al activity, a_{Al}, can be made using

$$\mu_{\mathrm{Al}} = \mu_{\mathrm{Al}}^0 + kTlna_{\mathrm{Al}}, \quad (4)$$

where k is the Boltzmann constant.

A Type III interface that matches (2×2) Ni(111) to (1×1) α-$Al_2O_3(0001)$, described elsewhere,[6] has been chosen because it has the lowest strain to commensuration. The mis-

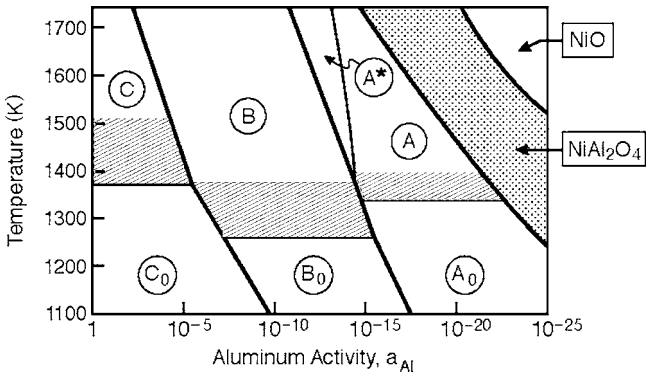

FIG. 1. Ni(111)/Al_2O_3(0001) interface phase diagram. Phases are as described in the text. The regions of $NiAl_2O_4$ and NiO are determined from the data of Ref. 23. The width of the cross-hatched region is based on a rough estimate of the error in phase transition temperatures (Ref. 27).

fit of the interface is about 3%. To ensure accurate calculations of W_{sep}, commensuration was obtained by minimizing the interfacial energy with respect to the Ni and Al_2O_3 bulk lattice constants.[14] The supercell includes six Ni layers, nine Al layers, and four oxygen layers. By not enforcing symmetry, all possible configurations were assessed for each Ni, Al, and O distribution at the interface. The bulk chemical potentials, $\mu_i^0(0)$, at absolute zero are determined from total energy computations. The procedure for determining the temperature dependences of the chemical potential have been described elsewhere.[6] The thermodynamic quantities required for this determination have been obtained from experimental measurements.[19] An estimation of the accuracy of these approximations in the context of interfacial phase diagrams[6,14,15] revealed that, while phase transition temperatures are not precise, trends in interfacial stability are reliable. For total-energy and force calculations, the exchange-correlation potential follows the generalized gradient approximation (GGA).[20] The plane wave method[21] with ultrasoft pseudopotentials[22] is employed to solve the Kohn-Sham equations. The energy cutoff for the plane-wave basis set is taken to be E_{cut}=400 eV. A $5\times5\times1$ uniform **k**-point sampling is taken over the Brillouin zone. At equilibrium, the total energy is minimized until the forces on all atoms fall below 20 meV/Å.

The calculated phase diagram for the interface is presented in Fig. 1 at temperatures relevant to applications of the Ni/Al_2O_3 interface (1100–1700 K). A total of seven phases have been found and denoted: A, A_0, A^*, B, B_0, C, and C_0. The phases occupy two temperature domains and three ranges of Al activity. Note that these are not phase diagrams in the usual materials science connotation, because actual phases and interfacial phases have been combined. Nevertheless, the representation provides a convenient visualization. In practice, the thermodynamic parameters are sufficiently accurate to enable the phase boundaries to be precisely located. Estimates of the uncertainty are used to incorporate a transition region between the high and low temperature phases (hatched area of Fig. 1). This region occurs at about 1300 K, independent of the activity. The corresponding interfacial structures for six of the phases are shown on Fig. 2

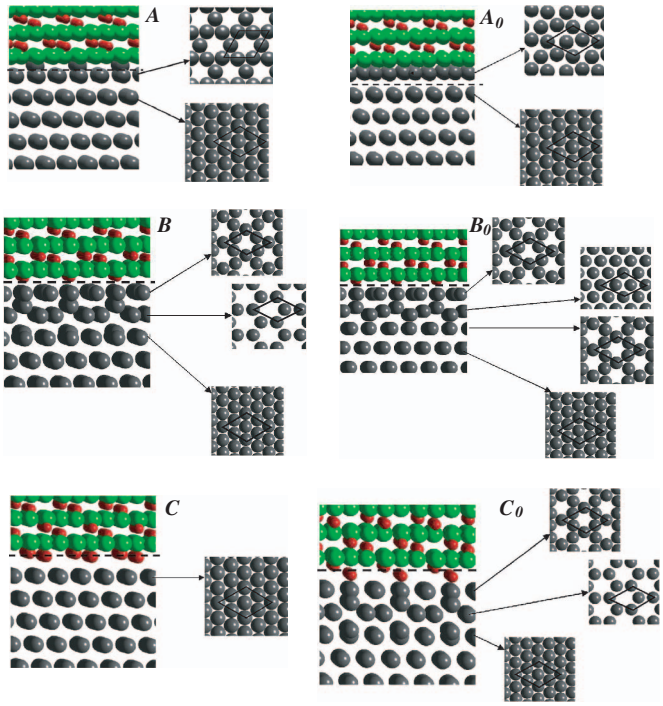

FIG. 2. (Color online) Atomic model for configuration A, A_0, B, B_0, C, and C_0: The gray (green) spheres represent the O, the small (red) Al, and the black Ni. The dashed line indicates the plane of minimum W_{sep}.

(the A^* phase is not included because it occupies such a small domain). As reported previously,[6] the phases at lowest Al activity (A, A_0, and A^*) have oxygen-terminated interfaces ($n_{Al}/n_O<2/3$), the phases at largest a_{Al} (C and C_0) are Al-terminated ($n_{Al}/n_O>2/3$), and those at intermediate a_{Al} (B and B_0) have stoichiometric interfaces ($n_{Al}/n_O=2/3$). The structures are generally consistent with the model terminations,[6] except that vacancies and corrugations are now in evidence, especially for the high temperature phases. The differences in the interfacial energies, γ_I, from that for the B phases, denoted $\Delta\gamma_I$, are plotted on Fig. 3. The plots are for two representative temperatures, 1200 K and 1600 K, as a function of the Al activity. The two different temperature ranges, above and below ~1300 K, are evident in Fig. 3. Evidently, the γ_I for the stoichiometric interfaces are larger than for the oxygen-rich or Al-rich interfaces. The relation between W_{sep}, γ_I, and the surface energies $\sigma_{Al_2O_3}$ and σ_{Ni} is given by

$$W_{sep} = \sigma_{Al_2O_3} + \sigma_{Ni} - \gamma_I. \quad (5)$$

The surface energies of O-terminated and 2Al-terminated Al_2O_3(0001) surfaces are larger than that for the stoichiometric Al_2O_3(0001) surface over the range of Al activities of interest.[24,25] These trends in both interfacial and surface energies yield smaller W_{sep} for the stoichiometric interfaces than for the O-rich and Al-rich interfaces, consistent with the results shown in Fig. 4.

To gain insight into these trends, we apply the electron localization function (ELF),[26] even though the characterization of atomic bonds in terms of ionic, covalent, or metallic

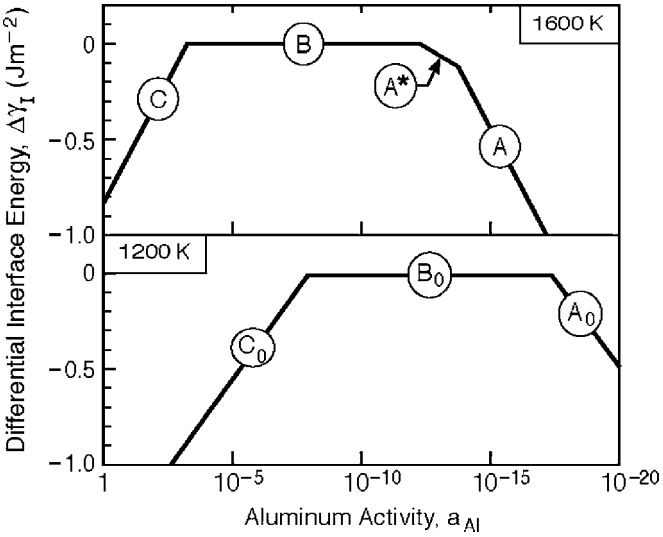

FIG. 3. Interfacial energies γ_I at 1200 K and 1600 K relative to the stoichiometric phases B_0 and B, respectively. The interfacial phases are denoted as in Figs. 1 and 2.

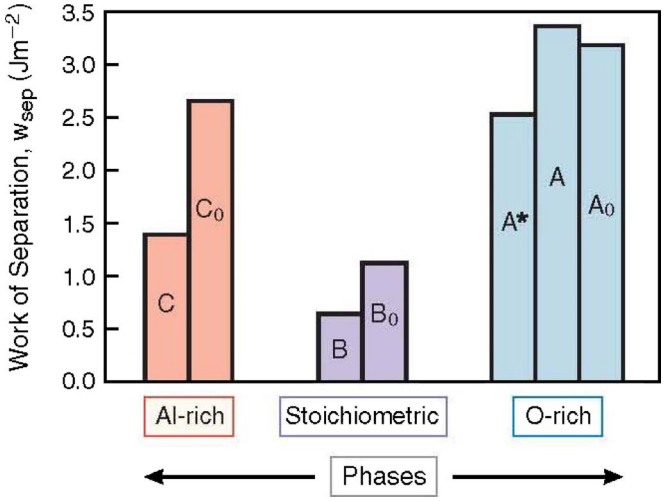

FIG. 4. (Color online) Works of separation W_{sep} for each interfacial phase as denoted in Figs. 1 and 2 and in the text.

is qualitative because of electron sharing between atoms. ELF suggests primarily ionic bonding between the Ni and O atoms. Accordingly, the O-rich interfaces are the strongest because of the bonding between Ni and O atoms across the interface. For phase A as shown in Fig. 2, this bonding is manifest as a small interfacial spacing of only 1.35 Å, with the outermost Ni atoms occupying the sites between the O atoms in the layer closest to the interface (outermost oxygen layer). This is consistent with stronger bonds typically implying smaller equilibrium interatomic spacings. The average bond length between Ni and O atoms is about 2.11 Å, close to the 2.09 Å found in bulk NiO. For phase A_0 as shown in Fig. 2, the Ni atoms of the outermost Ni layer occupy the Al sites of bulk Al_2O_3, and are close to the oxygen atomic plane. The bond length between the O and Ni atoms is 1.97 Å. The Ni atoms of the second Ni layer are located above the O atoms of the outermost oxygen layer, and the bond length between the O and Ni atoms is 1.98 Å.

For the Al-rich C-phases as shown in Fig. 2, the lowest W_{sep} entails separation between the outermost Al layers (denoted by the location of the dashed line in Fig. 2), because the resultant $Al_2O_3(0001)$ surface is at the ground-state (Al terminated, no dangling bond). This is reminiscent of bulk $Al_2O_3(0001)$, where the lowest W_{sep} also occurs between two Al layers. But in this case, the Ni/Al_2O_3 bonding has both similarities and differences with bulk Al_2O_3. Note that for separation between two Al layers, the bonds across the interface are broken between Al atoms and Ni atoms, between Al atoms and O atoms, and between Al atoms. The ELF analysis reveals primarily metallic bonding between Al and Ni at the interface, consistent with Ni_3Al-like bonding. Indeed, for phase C, the bond length between the Al atoms and the nearest Ni atoms (2.55 Å) is close to the 2.53 Å for bulk Ni_3Al. This is of course quite different from bulk Al_2O_3bonds. ELF indicates that the Al-O bonds across the interface are primarily ionic, similar to bulk Al_2O_3. The higher temperature phase C has a lower W_{sep}, perhaps because the two Ni layers closest to the interface exhibit considerable rumpling and more vacancies (less interfacial bonds per cross-sectional area).

The stoichiometric B phases are formed between the Al-terminated surface of $Al_2O_3(0001)$ and Ni(111). The plane of lowest W_{sep} (dashed line in Fig. 2) is between the outermost Al layer and the outermost Ni layer. The relatively low W_{sep} found in this case is likely due to the Al-terminated $Al_2O_3(0001)$ surface being the ground state, i.e., least reactive of the surface stoichiometries.

Experimental techniques capable of probing these high temperature phases include high resolution transmission electron microscopy. These studies require meticulous specimen preparation and specialized imaging capability. They are in progress, but not yet complete.[30] Should misfit dislocations be found, such features will be included in future extensions of the method.

An interfacial phase diagram has been computed for Ni/Al_2O_3 as a function of temperature and Al activity. The present computations embellish those reported[6] earlier, yielding a broader set of interfacial phases by allowing for vacancy formation as well as atomic mixing across the interface. Seven interfacial phases are identified, occupying two temperature domains (above and below about 1300 K), and three ranges of Al activity. The results corroborate the earlier finding that the interfacial stoichiometry is key to the magnitude of the work of separation, W_{sep}, with Al-rich and O-rich interfaces being stronger than stoichiometric interfaces. These results provide insight into the associated bonding mechanisms. The high strength of the O-rich phases (highest W_{sep}) derives from a primarily ionic bond between Ni and O atoms across the interface, reminiscent of NiO. The Al-rich phases are next in strength, arising from an interfacial mix of Ni_3Al-like and Al_2O_3-like bonding. The relative weakness of the stoichiometric interface is attributed to its dependence on the bond between Ni and the ground state Al_2O_3 surface.

The authors gratefully acknowledge AFOSR support from Grant No. FA9550-05-C-0039 and a grant from the DOD HPC resources from the Arctic Region Supercomputing Center, University of Alaska.

[1] N. P. Padture, M. Gell, and E. H. Jordan, Science **296**, 280 (2002).
[2] G. Levi, D. R. Clarke, and W. D. Kaplan, Interface Sci. **12**, 73 (2004).
[3] A. G. Evans, D. R. Mumm, J. W. Hutchinson, G. H. Meier, and F. S. Pettit, Prog. Mater. Sci. **46**, 505 (2001).
[4] A. G. Evans, J. W. Hutchinson, and Y. Wei, Acta Mater. **47**, 4093 (1999).
[5] F. Gaudette, S. Suresh, A. G. Evans, G. Dehm, and M. Ruhle, Acta Mater. **45**, 3503 (1997).
[6] W. Zhang, J. R. Smith, and A. G. Evans, Acta Mater. **50**, 3803 (2002).
[7] E. Saiz, R. M. Cannon, and A. P. Tomsia, Acta Mater. **47**, 4209 (1999); in *Ceramic Microstructure: Control at the Atomic Level*, edited by A. P. Tomsia and A. Glaeser (Plenum Press, New York, 1998).
[8] D. Chatain, L. Courdurier, and N. Eustathopoulos, Rev. Phys. Appl. **23**, 1955 (1988).
[9] J. G. Li, L. Coudurier, and N. Eustathopoulos, J. Mater. Sci. **24**, 1109 (1989).
[10] U. Alber, H. Mullejans, and M. Ruhle, Micron **30**, 101 (1999).
[11] W. Zhang, J. R. Smith, X.-G. Wang, and A. G. Evans, Phys. Rev. B **67**, 245414 (2003).
[12] R. M. Pilliar and J. Nutting, Philos. Mag. **16**, 181 (1967).
[13] C. Wan and M. Dupeux, J. Mater. Sci. **28**, 5079 (1993).
[14] X.-G. Wang and J. R. Smith, Phys. Rev. Lett. **95**, 156102 (2005).
[15] X.-G. Wang and J. R. Smith, Phys. Rev. B **70**, 081401(R) (2004); **68**, 201402 (2003); Wenqing Zhang, John R. Smith, and Xiao-Gang Wang, *ibid.* **70**, 024103 (2004).
[16] C. G. Van de Walle and J. Neugebauer, Phys. Rev. Lett. **88**, 066103 (2002).
[17] K. Reuter and M. Scheffler, Phys. Rev. B **65**, 035406 (2002).
[18] M. W. Finnis, A. Y. Lozovoi, and A. Alavi, Annu. Rev. Mater. Res. **35**, 167 (2005).
[19] *CRC Handbook of Chemistry and Physics*, edited by R. Weast and M. J. Astle (CRC Press, Inc., Boca Raton, FL, 1978).
[20] J. P. Perdew and Y. Wang, Phys. Rev. B **45**, 13244 (1992).
[21] G. Kresse and J. Hafner, Phys. Rev. B **49**, 14251 (1994).
[22] D. Vanderbilt, Phys. Rev. B **41**, 7892 (1990).
[23] K. P. Trumble and M. Ruhle, Acta Metall. Mater. **39**, 1915 (1991).
[24] Xiao-Gang Wang, Anne Chaka, and M. Scheffler, Phys. Rev. Lett. **84**, 3650 (2000).
[25] E. A. Soares, M. A. Van Hove, C. F. Walters, and K. F. McCarty, Phys. Rev. B **65**, 195405 (2002).
[26] B. Silvi and A. Savin, Nature **371**, 683 (1994).
[27] In this estimate, the local vibration behaviors of the interfaces are determined by their bonding properties (Ni_3Al for Phase C_0, C, B_0 and B; NiO for Phase A_0 and A). Based on the Einstein model, the difference in interfacial energies due to vibrations is taken as, $\Delta F_s(T) \sim kT\Delta N_{Ni} \ln[2 \sinh(h\nu/kT)]$. The phonon frequency ν was equated to the highest frequency of the local vibrations, and taken from Refs. 28 and 29. This expression yields the upper bound to the cross-hatched region. The lower bound is found with $\Delta F_s(T)=0$.
[28] Y. Wang, Z.-K. Liu, and L.-Q. Chen, Acta Mater. **52**, 2665 (2004).
[29] S. Y. Savrasov and G. Kotliar, Phys. Rev. Lett. **90**, 056401 (2003).
[30] M. Ruehle (private communication).